AMERICAN SOCIETY FOR MICROBIOLOGY | Applied and Environmental Microbiology

Spotlight Selection | Molecular and Cellular Biology | Full-Length Text

An *Azospirillum brasilense* chemoreceptor that mediates nitrate chemotaxis has conditional roles in the colonization of plant roots

Elena E. Ganusova,[1] Matthew H. Russell,[1] Siddhi Patel,[1] Terry Seats,[1] Gladys Alexandre[1]

AUTHOR AFFILIATION See affiliation list on p. 16.

ABSTRACT Motile plant-associated bacteria use chemotaxis and dedicated chemoreceptors to navigate gradients in their surroundings and to colonize host plant surfaces. Here, we characterize a chemoreceptor that we named Tlp2 in the soil alphaproteobacterium *Azospirillum brasilense*. We show that the Tlp2 ligand-binding domain is related to the 4-helix bundle family and is conserved in chemoreceptors found in the genomes of many soil- and sediment-dwelling alphaproteobacteria. The promoter of *tlp2* is regulated in an NtrC- and RpoN-dependent manner and is most upregulated under conditions of nitrogen fixation or in the presence of nitrate. Using fluorescently tagged Tlp2 (Tlp2-YFP), we show that this chemoreceptor is present in low abundance in chemotaxis-signaling clusters and is prone to degradation. We also obtained evidence that the presence of ammonium rapidly disrupts Tlp2-YFP localization. Behavioral experiments using a strain lacking Tlp2 and variants of Tlp2 lacking conserved arginine residues suggest that Tlp2 mediates chemotaxis in gradients of nitrate and nitrite, with the R159 residue being essential for Tlp2 function. We also provide evidence that Tlp2 is essential for root surface colonization of some plants (teff, red clover, and cowpea) but not others (wheat, sorghum, alfalfa, and pea). These results highlight the selective role of nitrate sensing and chemotaxis in plant root surface colonization and illustrate the relative contribution of chemoreceptors to chemotaxis and root surface colonization.

IMPORTANCE Bacterial chemotaxis mediates host-microbe associations, including the association of beneficial bacteria with the roots of host plants. Dedicated chemoreceptors specify sensory preferences during chemotaxis. Here, we show that a chemoreceptor mediating chemotaxis to nitrate is important in the beneficial soil bacterium colonization of some but not all plant hosts tested. Nitrate is the preferred nitrogen source for plant nutrition, and plants sense and tightly control nitrate transport, resulting in varying nitrate uptake rates depending on the plant and its physiological state. Nitrate is thus a limiting nutrient in the rhizosphere. Chemotaxis and dedicated chemoreceptors for nitrate likely provide motile bacteria with a competitive advantage to access this nutrient in the rhizosphere.

KEYWORDS *Azospirillum*, chemotaxis, chemoreceptor, nitrate, PGPR

Azospirillum brasilense are alphaproteobacteria capable of nitrogen fixation under free-living conditions. These bacteria have been reported to colonize the roots and promote the growth of plants from over 113 species that span 35 botanical families (1). Their plant growth-promoting activities are related to phytohormone, siderophore, secondary metabolites production, and nitrogen fixation, a set of properties that make these bacteria good candidates as biological fertilizers (2).

Editor Gemma Reguera, Michigan State University, East Lansing, Michigan, USA

Address correspondence to Gladys Alexandre, galexan2@utk.edu.

The authors declare no conflict of interest.

See the funding table on p. 16.

Received 17 April 2024
Accepted 26 April 2024
Published 22 May 2024

An effective boost of plant growth by the inoculation of Azospirilla depends on robust colonization of the root surfaces (3). Detecting and navigating toward chemical compounds released by plant roots in their surroundings are essential for root surface colonization, and it depends on bacterial chemotaxis (4, 5). The signal transduction pathway governing bacterial chemotaxis is prevalent across sequenced microbial genomes and is particularly enriched in soil metagenomes, likely due to its ecological advantage for motile organisms (6). During chemotaxis, chemoreceptors detect chemical cues, transmitting this information to cytoplasmic proteins through phosphorelay between associated soluble chemotaxis-signaling proteins. These events modulate the direction of flagellar motor rotation, influencing swimming behavior (7). In Archaea and Bacteria, chemotaxis receptors (or chemoreceptors) are organized as polar clusters of large arrays of interacting trimers of chemoreceptor dimers, with this organization enhancing sensitivity and response range (8–10). The majority of prototypical transmembrane chemotaxis chemoreceptors possess an N-terminal, periplasmic sensory domain followed by a conserved cytoplasmic C-terminal signaling domain that interacts with other chemoreceptors and chemotaxis-signaling proteins to form stable arrays (6, 11). The sensory functions of most bacterial chemoreceptors have been identified through a combination of genetic and biochemical approaches, as well as comparative genomics, though most chemoreceptors have sensory specificity that remains uncharacterized (12). *A. brasilense* bacteria possess a versatile oxidative metabolism and can perform diazotrophy under microaerobic (~3–5 µM dissolved oxygen) conditions (13). These motile bacteria grow best with and exhibit preferential chemotaxis toward organic acids and, to a lesser extent, sugar. They prefer ammonium chloride as an organic nitrogen source and can use nitrate and some amino acids as nitrogen sources for growth (14). The analysis of the complete *A. brasilense* genome sequence revealed the presence of four potential chemotaxis-like signal pathways, two of which function to control flagella-mediated chemotaxis (15), and 51 chemotaxis receptors (16). The two essential chemotaxis pathways in *A. brasilense*, Che1 and Che4, mediate chemotaxis by integrating sensory cues from two spatially distinct membrane-bound signaling arrays in which Che1 and Che4 proteins mix and transmit chemotaxis signals to the flagellar motors (17). The annotated genome sequence of *A. brasilense* suggests that chemoreceptors employ seven different ligand binding domain (LBD) types for signal sensing including the 4-helix bundle (4HB) (twelve chemoreceptors), CACHE (nine chemoreceptors), PAS (five chemoreceptors), Protoglobin (three chemoreceptors), helical bimodular (HBM) (one chemoreceptor), and twenty-one receptors with LBD of unknown type (18).

Only four chemoreceptors have been characterized in *A. brasilense* through mutant analysis and behavioral assays: Tlp1 (19, 20), AerC (21), Aer (22), and Tlp4b (23). Except for AerC and Aer, which both use FAD as cofactors for sensing redox metabolism, the sensory specificity of *A. brasilense* chemoreceptors is not known. The present study reports the characterization of the chemoreceptor Tlp2 (transducer-like protein 2) through mutagenesis and behavioral assays. The LBD of the Tlp2 protein was not previously annotated. AlphaFold model predicts that Tlp2 has a prototypical transmembrane topology exposing a conserved periplasmic N-terminal domain related to the 4HB family. Here, we provide evidence that *tlp2* is regulated as part of the RpoN and NtrC regulons, which control nitrogen metabolism, including nitrogen fixation and nitrate assimilation in *A. brasilense* (24, 25). Using mutagenesis, fluorescence microscopy, and behavioral assays, we show that Tlp2 is present in low abundance, is prone to degradation, and likely mediates chemotaxis toward nitrate and nitrite. We also show that the contribution of Tlp2 to the colonization of plant roots depends on the host plant tested, suggesting this low abundance and unstable chemoreceptor may play a role in host plant root selection.

RESULTS

The sensory domain of Tlp2 is predicted to form a 4-HB and is conserved in closely related alphaproteobacteria

The sequence corresponding to *tlp2* (WP_035678663.1) was originally identified from an *A. brasilense* Sp7 genomic library and is predicted to encode a chemoreceptor with an N-terminal periplasmic putative sensory domain or LBD (142 amino acids), which is flanked by two transmembrane helices, as well as a large cytoplasmic conserved domain with homology to the signaling domains of other chemotaxis receptors (https://mistdb.com/mist/genes/GCF_001315015.1-AMK58_RS19255). A PSI-BLAST search of the nonredundant (nr) NCBI database using the periplasmic sensing domain of Tlp2 as a query indicated that this putative sensory domain is conserved and present in other chemotaxis-like receptor sequences from the genomes of closely related Rhodospirillaceae, Pseudobdellovibrionaceae, Geminicoccaceae, and Azospirillaceae families. The PHI-BLAST search returned 203 hits of the sequences with similarity ranging from 99.35% to 43.97% identity in amino acid sequences. About 43% of the identified species belonged to the genus *Azospirillum*. Most bacterial species (94.5%) that harbor these homologs correspond to isolates that dwell in soils and sediments, suggesting a function for this sensory domain in these habitats. A multiple sequence alignment of the Tlp2 LBD to closely related LBD of bacterial species other than *Azospirillum* showed five conserved regions with conserved arginine residues present in each region (Fig. S1; Fig. 1A). An AlphaFold model of the LBD structure suggests that its fold is similar to the 4HB domain (Fig. 1B).

The *tlp2* gene is part of the RpoN and NtrC regulons

Analysis of the promoter region of *tlp2* revealed a consensus binding sequence for NtrC (TGCACCCTCATGAAGACA) and RpoN (Sigma 54) (TGGAACGATTTAAC ACTTCG) transcriptional regulatory proteins (26). NtrC regulates RpoN-dependent promoters under conditions of nitrogen limitation (25, 27), suggesting that the expression of *tlp2* may be regulated by the availability of nitrogen sources. We tested the activity of the *tlp2* promoter (P_{tlp2}) in the *A. brasilense* parent strain (Sp7, herein defined as WT strain) by using a translational fusion to the promoterless *gusA* gene in the broad-host range pFUS1 vector (28) under diverse growth conditions. The expression driven by P_{tlp2} was not detected when tested in an *A. brasilense* mutant derivative lacking *rpoN* [*rpoN::Km* (24), herein *rpoN*], and it was partially active in a mutant derivative lacking *ntrC* [*ntrC::Tn5* (29), herein, *ntrC*] (Fig. 2A). Consistent with the NtrC-RpoN regulation, promoter activity of *tlp2* was about three times higher when *A. brasilense* cells were incubated for 24 hours under conditions of nitrogen fixation (Fig. 2A) compared to incubation with supplemental nitrogen (Fig. 2B). When cells were grown in the presence of nitrate, the activities of both P_{rpoN} and P_{tlp2} were higher when cells were grown without shaking to limit aeration; however, this was not observed in the presence of ammonium chloride (Fig. 2B).

To further characterize the effect of nitrate and ammonium on P_{tlp2} activity, we first grew cells under conditions of nitrogen fixation (no source of nitrogen added and no aeration) to induce promoter activity and then added either ammonium or nitrate to the medium and incubated the cultures for 6 hours (Fig. 2C). Spiking the medium with ammonium chloride or sodium nitrate led to a significant reduction in the activity of both *tlp2* and *rpoN* promoters compared to nitrogen fixation conditions (Fig. 2C). The P_{tlp2} promoter is thus maximally induced under conditions of nitrogen fixation, and the presence of a nitrogen source reduced its activity. We further found that the reduction of P_{tlp2} activity is dependent on nitrate concentration, with 2 mM nitrate producing the lowest activity (Fig. 2D). We used the promoter region of *nap*A encoding periplasmic nitrate reductase (P_{napA}) as a positive control since *napA* expression depends on nitrate concentration in *A. brasilense* (30). In contrast, the promoter activity of *tlp2* remained

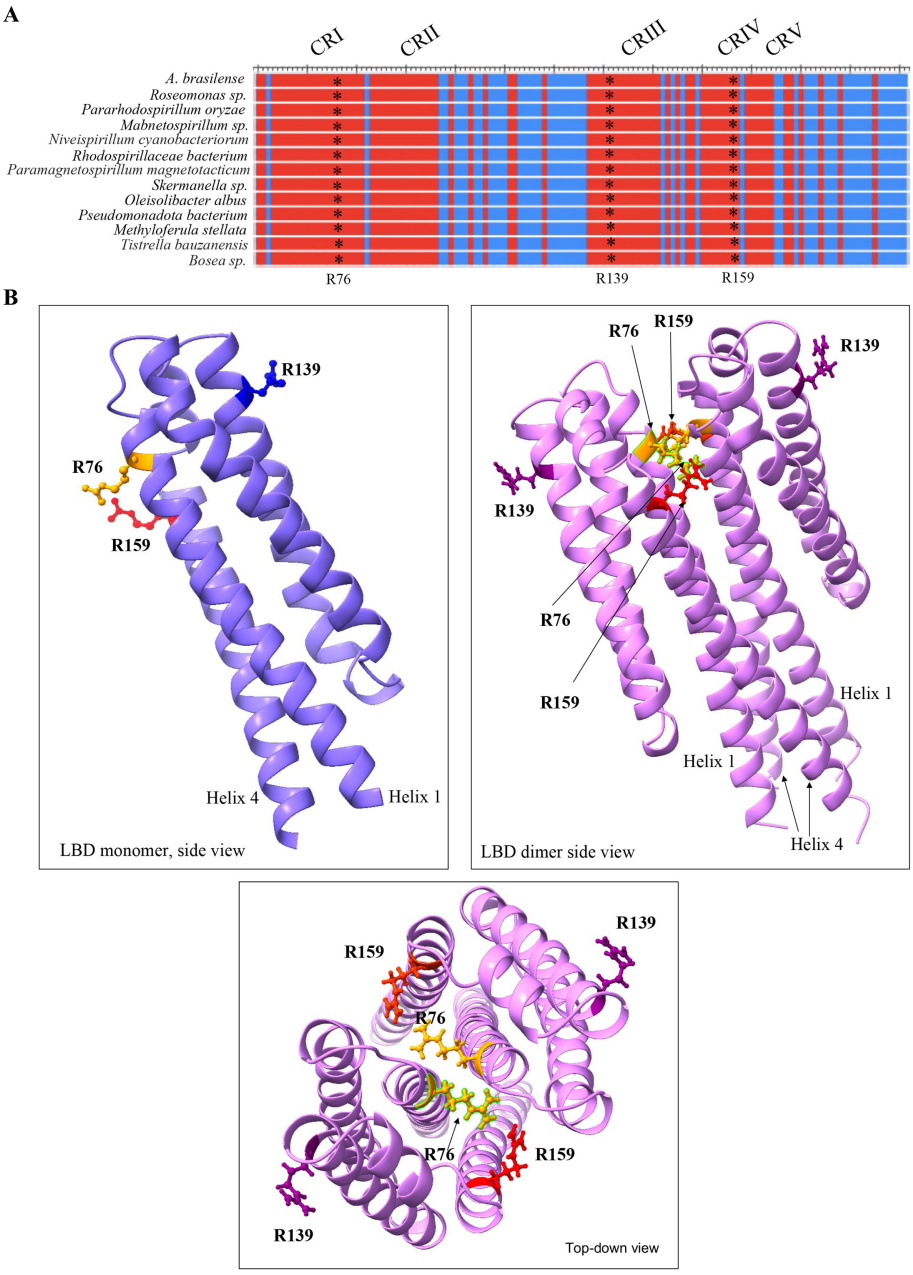

FIG 1 Sequence conservation in the LBD of chemoreceptor homologs of Tlp2. (A) Alignment of Tlp2 LBD protein sequences; red color indicates conserved amino acid sequences and blue color indicates non-conserved amino acid sequences. (B) AlphaFold-predicted structure of Tlp2 LBD (LBD monomer, left panel; LBD dimer, right panel; relative localization of the conserved arginine residues, bottom panel) indicating localization of the conserved arginine residues R76, R139, and R159 analyzed here.

low in ammonium regardless of the concentration and was not detected at all in the presence of 20 mM ammonium (Fig. 2D).

Tlp2 mediates chemotaxis toward nitrate, with the conserved R159 residue essential for this function

To characterize the role of Tlp2 in *A. brasilense* chemotaxis responses, we constructed a mutant derivative using deletion of the *tlp2* open reading frame, followed by insertion of an antibiotic resistance cassette and replacement by allelic exchange, to produce a

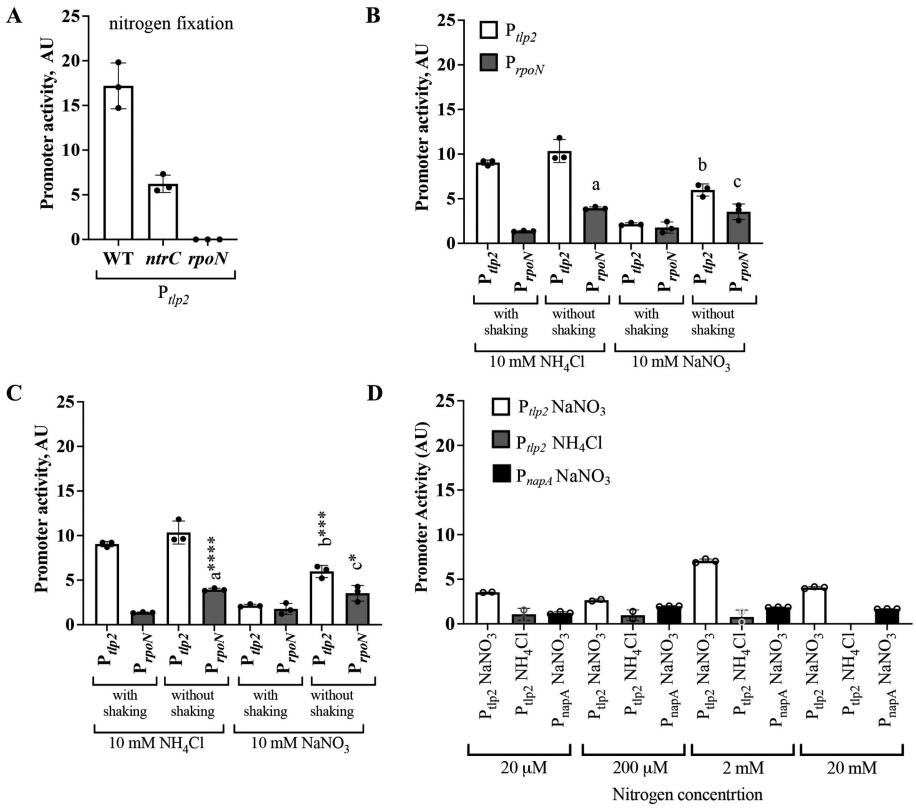

FIG 2 *tlp2* belongs to RpoN-NtrC regulon and its promoter activity is induced in the nitrogen starvation conditions. (A) Promoter activity of *tlp2* is decreased in the *ntrC* mutant strain and not detected in the *rpoN* mutant strain [****P = 0.0001 (by Student's *t*-test)]. (B) Promoter activity of *tlp2* and *rpoN* with shaking and without shaking in the medium with 10 mM NH_4Cl or $NaNO_3$ [significant difference is indicated: a—*rpoN* promoter activity in comparison with shaking vs no shaking in the medium with NH_4Cl (****P = 0.0001), b—*tlp2* promoter activity in comparison with shaking vs no shaking in the medium with $NaNO_3$ (***P = 0.001), and c—*rpoN* promoter activity in comparison with shaking vs no shaking in the medium with $NaNO_3$ (*P = 0.1, by Student's *t*-test)]. (C) Promoter activity of *tlp2* and *rpoN* in the nitrogen fixation condition and after 6 hours spike with 10 mM NH_4Cl or $NaNO_3$ [significant difference is indicated: a—*rpoN* promoter activity in comparison with shaking in 10 mM NH_4Cl (****P = 0.0001), b—*tlp2* promoter activity in comparison with shaking in 10 mM $NaNO_3$ (***P = 0.001, by Student's *t*-test), and c—*rpoN* promoter activity in comparison with shaking in 10 mM $NaNO_3$ (*P = 0.1, by Student's *t*-test)]. (D) Promoter activity of *tlp2* and *napA* in the media with various nitrate and ammonium concentrations.

Δ*tlp2* strain. Aerotaxis, or taxis in a gradient of oxygen, is one of the strongest behavioral responses in *A. brasilense* as it allows cells to find niches that are optimal for their microaerobic metabolism (14). There was no difference in the aerotaxis response of Δ*tlp2* in comparison with the WT in a spatial gradient assay for aerotaxis (Fig. S2A). Given the profiles of expression of P_{tlp2}, we next tested chemotaxis in spatial gradients of different nitrogen sources (Fig. S2B through F; Fig. 3). Under conditions of nitrogen fixation, the *Δtlp2* mutant carrying an empty vector (Δ*tlp2* ev) displayed reduced chemotaxis relative to the WT strain carrying an empty vector (WT ev), with the chemotaxis defect rescued by expressing the parental *tlp2* from a broad host range vector (Δ*tlp2* $Tlp2^{WT}$) (Fig. 3A).

We also compared the chemotaxis of WT ev, Δ*tlp2* ev, and Δ*tlp2* $Tlp2^{WT}$ with that of Δ*tlp2* strains expressing variants of Tlp2, in which the conserved R76, R139, or R159 residues were replaced with alanine (Δ*tlp2* $Tlp2^{R76A}$, Δ*tlp2* $Tlp2^{R139A}$, and Δ*tlp2* $Tlp2^{R159A}$) (Fig. 3; Fig. S2). The Δ*tlp2* ev strain and mutant complemented strain Δ*tlp2* $Tlp2^{R159A}$, but not the other variants, formed chemotaxis rings of smaller sizes compared to WT ev and Δ*tlp2* $Tlp2^{WT}$ in the presence of 5 mM ammonium chloride (Fig. S2B). However, the strains also exhibited a growth defect under these conditions (Fig. S2C), suggesting

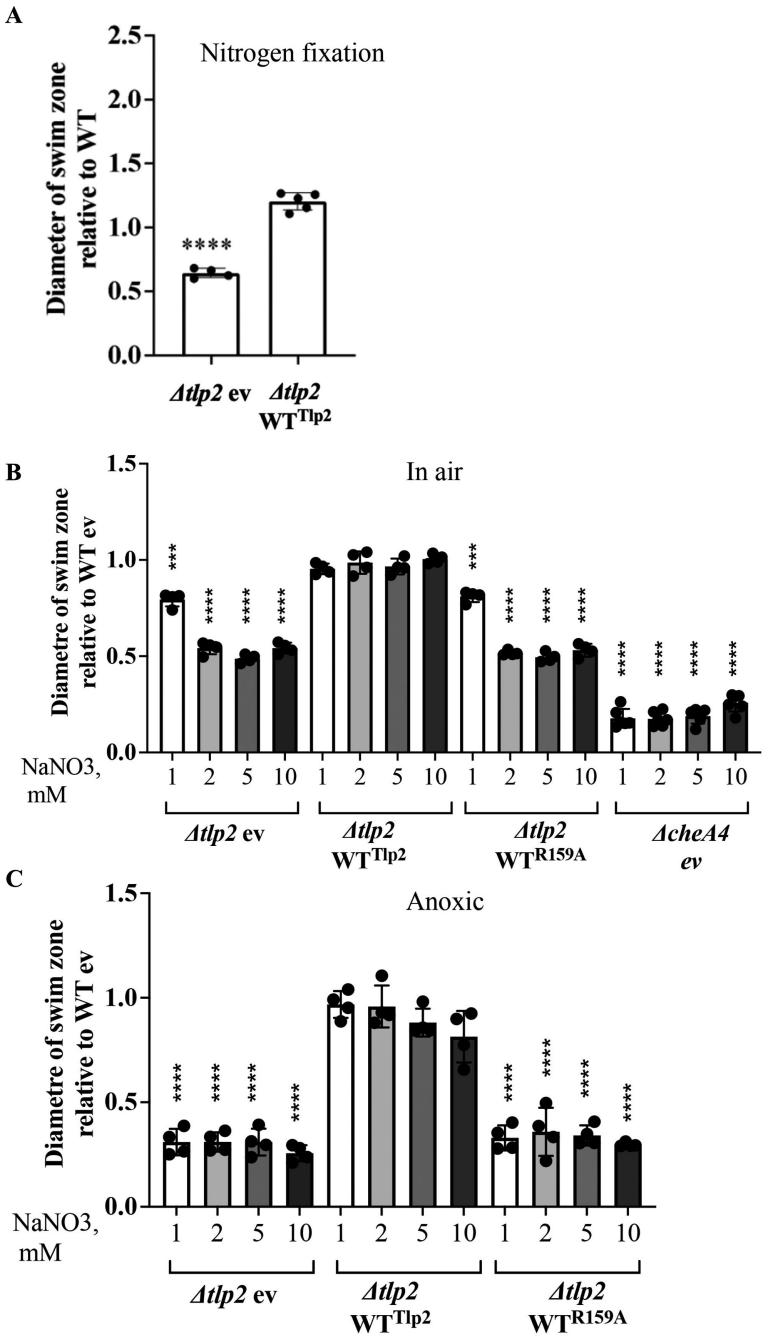

FIG 3 Deletion of *tlp2* affects the chemotactic behavior of *A. brasilense*. (A) Chemotaxis behavior of Δ*tlp2* ev and Δ*tlp2* Tlp2^{WT} normalized to WT ev under conditions of nitrogen fixation conditions (****P = 0.0001, by Student's *t*-test). (B) Chemotaxis behavior of Δ*tlp2* ev, Δ*tlp2* Tlp2^{WT}, Δ*tlp2* Tlp2^{R159A}, and *DcheA4* ev strains normalized to WT ev in the medium with 1, 2, 5, and 10 mM $NaNO_3$ and 37.5 mM malate (MMAB-based medium) in the presence of oxygen (***P = 0.001 and ****P = 0.0001, by Student's *t*-test). (C) Chemotaxis behavior of Δ*tlp2* ev, Δ*tlp2* Tlp2^{WT}, and Δ*tlp2* Tlp2^{R159A} strains normalized to WT ev in the medium with 1, 2, 5, and 10 mM $NaNO_3$ and 37.5 mM malate (MMAB-based medium) in the anoxic conditions.

the differences observed are due to growth impairment since growth contributes to the formation of rings in the soft agar plate assay.

In the presence of nitrate, there was no difference in the growth of the tested strains (Table S1). Under aerobic conditions, only Δ*tlp2* ev and Δ*tlp2* Tlp2^{R159A} (Fig. 3B; Fig. S2D)

displayed a significant reduction in the size of chemotaxis rings compared to WT ev and the Δ*tlp2* Tlp2^{WT} at concentrations above 1 mM. The chemotaxis defects of Δ*tlp2* ev and Δ*tlp2* Tlp2^{R159A} toward nitrate were concentration-dependent, consistent with a defect in the sensing of nitrate (Fig. 3B). We also tested the behavior of a Δ*cheA*4 mutant strain that is chemotaxis null (15) and found that the Δ*cheA4* formed smaller ring sizes compared to the Δ*tlp2* ev and the Δ*tlp2* Tlp2^{R159A}, regardless of the concentration of nitrate (Fig. 3B). This observation suggests residual chemotaxis to nitrate in the absence of Tlp2 and the existence of another chemoreceptor(s) mediating chemotaxis to nitrate.

We also tested chemotaxis toward nitrite and found similar defects for Δ*tlp2* ev and Δ*tlp2* Tlp2^{R159A}, but there was no defect detected with the other two variants (Fig. S2E). We confirmed the defect in chemotaxis in the Δ*tlp2* ev and the Δ*tlp2* Tlp2^{R159A} is related to nitrate and not the sodium salt by testing responses to potassium nitrate and found similar patterns (Fig. S3). Similarly, the defect in nitrate chemotaxis occurred with different carbon sources and produced similar behavioral patterns for the strains tested: Δ*tlp2* ev and Δ*tlp2* Tlp2^{R159A} displayed a significant chemotaxis defect compared to the WT ev that was restored in the Δ*tlp2* Tlp2^{WT} (Fig. S4).

A. brasilense can use nitrate as an alternative electron acceptor in the absence of oxygen and displays chemotaxis that depends on growth under these conditions (14). To further validate that Tlp2 contributes to sensing nitrate gradients, we also tested chemotaxis in the presence of various concentrations of $NaNO_3$ under anoxic conditions and found a consistent defect for Δ*tlp2* ev and Δ*tlp2* Tlp2^{R159A}, regardless of the concentration of nitrate used (Fig. 3C). The similar effect seen for various concentrations of nitrate under these anaerobic conditions probably reflects the fact that the differences measured are the consequences of sensing (or not) the nitrate gradient: in the soft agar assay, strains create a nitrate gradient through metabolism at the point of inoculation, so strains that cannot navigate a nitrate gradient will remain at the inoculation site and fail to grow outward from the inoculation point regardless of the nitrate concentration. Δ*tlp2* Tlp2^{R76A} and Δ*tlp2* Tlp2^{R139A} did not show any defect in their response to nitrate under anoxic conditions and behaved similar to the WT ev strain (Fig. S2F). Together, the data support the hypothesis that Tlp2 contributes to sensing nitrate and to a lesser extent, nitrite, with the conserved R159 being essential for Tlp2 function in mediating nitrate and nitrite chemotaxis.

Tlp2-YFP polar localization with other chemotaxis proteins is enhanced in the presence of nitrate or under nitrogen fixation conditions

If Tlp2 functions as part of the chemotaxis signaling machinery of *A. brasilense*, then it should localize at the cell poles in a chemotaxis signaling protein-dependent manner (17). We expressed a Tlp2-YFP fusion from the native *tlp2* promoter on a low copy plasmid (pRH005) and first demonstrated that the Tlp2-YFP fusion was functional by showing that this construct could restore chemotaxis to a Δ*tlp2* strain when assaying in a spatial gradient assay for chemotaxis and compared to a strain expressing an empty vector (Fig. S5). When grown in the presence of ammonium (10 mM) or nitrate (10 mM), Tlp2-YFP was diffuse, and no distinct fluorescent foci were detected, regardless of aeration status (shaking vs non-shaking cultures) (Fig. 4A through D). *A. brasilense* accumulates polyhydroxybutyrate (PHB) granules in the presence of nitrate (31), which is likely the reason for the differences seen in the morphology of cells grown in ammonium chloride vs sodium nitrate. These data suggested that Tlp2-YFP is either not clustering with the chemotaxis signaling arrays or is present at low abundance under these conditions.

Next, we used the information from the P_{tlp2} activity (Fig. 2B) to further characterize the Tlp2-YFP subcellular localization. When cells were incubated without a nitrogen source and under conditions of nitrogen fixation for 24 hours, we observed dim polar localization of Tlp2-YFP in ~1.4% (n = 477 cells) of the cells (Fig. 4E). No polar localization of YFP was detected under all tested conditions when the Δ*tlp2* strain carried an empty plasmid (Fig. S6). Transfer from the nitrogen fixation conditions to a medium

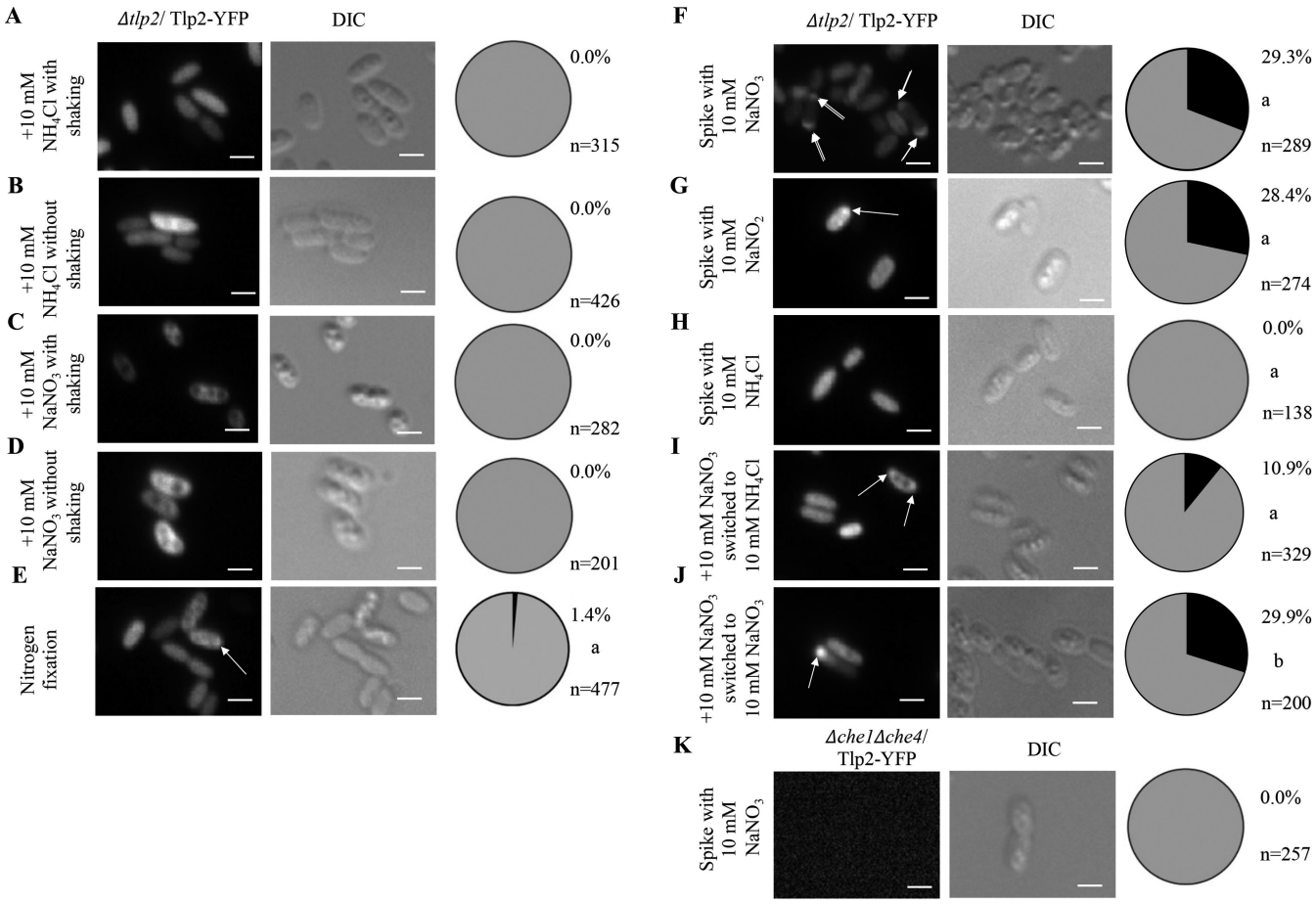

FIG 4 Polar localization of Tlp2-YFP in Δ*tlp2* cells depends on the presence of the nitrogen source. Tlp2-YFP expressed in the Δ*tlp2* strain is diffused in the medium with 10 mM ammonium with (A) or without shaking (B). Tlp2-YFP expressed in the Δ*tlp2* strain is diffused in the medium with 10 mM nitrate with (C) or without shaking (D). Nitrogen starvation slightly induces polar localization of Tlp2-YFP (E). Localization of Tlp2-YFP in Δ*tlp2* strain after a spike of the nitrogen-free medium with 10 mM of nitrate (F), 10 mM nitrite (G), or 10 mM ammonium (H). Localization of Tlp2-YFP in Δ*tlp2* strain after spike of the nitrogen-free medium with 10 mM of nitrate and subsequent wash and substitution of nitrate with 20 mM ammonium (1 hour) (I) or 10 mM nitrate (J). Localization of Tlp2-YFP in Δ*che1*Δ*che4* chemotaxis "null" mutant after a spike of the nitrogen-free medium with 10 mM of nitrate (K). The scale bar is 1 mm. Quantification of the fraction of the cells with diffuse (gray color) and polar (black color) localization of Tlp2-YFP is presented on the right of the fluorescent images. *n* represents the number of quantified cells. The *n* value next to each pie chart indicates the sample size. The *z*-score test was used to determine the significance of the fluorescent-focus localization of Tlp2-YFP in the Δ*tlp2* mutant in comparison with nitrogen fixation [a—significant in comparison with nitrogen fixation conditions (*P* is <0.00001), b—significant in comparison between ammonium and nitrate medium, *P* is <0.00001].

supplemented with 10 mM nitrate (spike for 6 hours) increased the number of cells detected with polar localization up to 29.3% (*n* = 289 cells), although the fluorescent foci remained dim (Fig. 4F). A similar increase in the polar localization of Tlp2-YFP occurred in the presence of nitrite (Fig. 4G). Spiking with 10 mM ammonium for 6 hours after nitrogen fixation conditions caused diffuse localization of Tlp2-YFP, and Tlp2-YFP polar foci were not detected (Fig. 4H).

In contrast, when cells were transferred from the nitrogen fixation conditions to a medium with 10 mM ammonium or with 10 mM nitrate for 1 hour, the fraction of cells displaying Tlp2-YFP polar foci decreased from 29.9% (*n* = 200 cells) to 10.9% (*n* = 329 cells) in the presence of ammonium compared to the presence of nitrate (Fig. 4I and J). The fraction of cells with polar Tlp2-YFP localization transferred from nitrate to nitrate did not change significantly, as expected (Fig. 4I). The polar localization of Tlp2-YFP was abolished in a Δ*che1*Δ*che4* mutant strain background (Fig. 4K), consistent with Tlp2-YFP joining chemotaxis signaling arrays (17, 23). These observations indicate

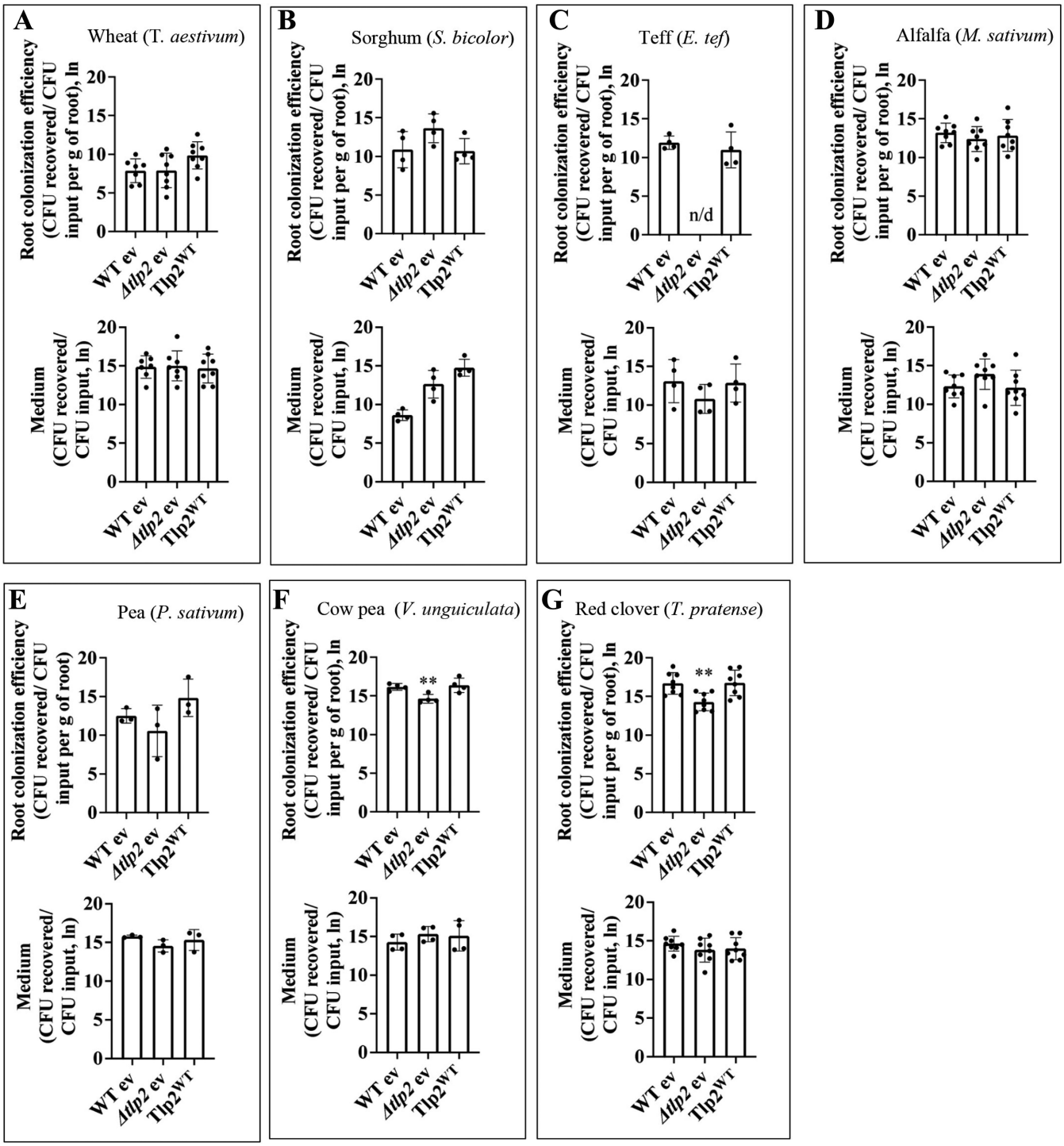

FIG 5 Root colonization assay with WT, Δ*tlp2* ev, and Δ*tlp2* Tlp2^{WT}. (A) Wheat roots (*Triticum aestivum*), (B) sorghum roots (*Sorghum bicolor*), (C) teff roots (*Eragrostis tef*), (D) alfalfa (*Medicago sativa*) roots, (E) pea roots (*Pisum sativum*), (F) cowpea roots (*Vigna unguiculata*) roots, and (G) red clover roots (*Trifolium pratense*) roots. The upper panel indicates the CFU recovered from the roots, and the bottom panel indicates the CFU from the root surrounding medium. Asterisks indicate statistically significant differences compared with the wild-type (WT ev) strain [**P = 0.01 (by Student's t-test)].

that brief exposure to ammonium is sufficient to reduce the fraction of cells detected with fluorescent Tlp2-YFP foci. Together, the data are consistent with the pattern of *tlp2* promoter activity and further suggest that the presence of ammonium, but not nitrate, destabilizes the polar localization of Tlp2-YFP as fluorescent foci.

We next used Western blot to probe the abundance and potential stability of Tlp2-YFP as a function of the nitrogen source present in the medium with conditions like those used in Fig. 3A and B. In all conditions and repeated experiments, there was significant smearing and degradation of Tlp2-YFP, including for high-molecular-weight species of unknown identity, but that could correspond to higher-molecular-weight Tlp2-YFP complexes (Fig. S7). These degradation and smearing products did not appear to correspond to an issue with the antibody since strains expressing YFP alone from the same vector did not produce any smear or similar pattern of degradation (Fig. S7A). The fraction of folded Tlp2-YFP was similar regardless of the conditions tested (Fig. S7B). These data indicate that multiple degradation products are produced when Tlp2-YFP is expressed from a low-copy plasmid, suggesting instability of the construct. Degradation and smearing did not change when cells were transferred from nitrogen fixation conditions to a medium with ammonium or various concentrations of nitrate for 6 hours (Fig. S7C). These observations suggest that the change in the abundance of fluorescent foci of Tlp2-YFP detected after 6-hour incubation with ammonium or nitrate is more likely caused by changes in the clustering of Tlp2-YFP within the polar chemotaxis signaling clusters rather than changes in protein degradation.

Tlp2 is not essential for the root colonization of cereals but indispensable for the root colonization of some legumes

Given the role of Tlp2 in chemotaxis, we next tested the contribution of this chemoreceptor to root colonization of various plants by comparing WT ev to Δ*tlp2* ev and Δ*tlp2* Tlp2^{WT} in colonization of plant roots germinated under sterile conditions. No statistical differences were detected in the concentration of cells recovered from the roots colonized by the wild type, the mutant, or complemented strains when tested on wheat (Fig. 5A), sorghum (Fig. 5B), alfalfa (Fig. 5D), and pea (Fig. 5E), while the population recovered from the media was also not different from the inoculum. This suggests that there was no significant change in the growth or viability of the strains under these conditions. One exception is for strains inoculated into sorghum, where the population of Δ*tlp2* ev and Δ*tlp2* Tlp2^{WT} recovered from the media relative to the inoculum was increased compared to WT ev. One possibility is that the environment influenced by sorghum roots, for example through the root exudates composition, differentially affected the strains inoculated. It is not clear at this point whether the differences were due to growth, chemotaxis, or colonization abilities or a combination of these effects. In contrast, the Δ*tlp2* ev strain was severely defective in the colonization of teff roots (Fig. 5C), and to a lesser extent cowpea (Fig. 5F) and red clover (Fig. 5G) roots, with the defects being rescued by expressing Tlp2^{WT}. The concentration of cells recovered from the media was not significantly different from the inoculum, suggesting there was no major change in growth or viability. Together, the findings indicate that the contribution of Tlp2 to root surface colonization depends on the plant considered, with both colonization of some cereals (teff) as well as some legumes (cowpea and red clover) requiring functional Tlp2 for wild-type level root surface colonization. No major effect on growth or viability was detected, suggesting that nitrate chemotaxis mediates these differences rather than a growth defect such as the one detected on ammonium above.

DISCUSSION

Here, we describe an *A. brasilense* chemoreceptor Tlp2, which mediates chemotaxis in gradients of nitrate, and found that this function has varied contributions to the colonization of plant roots, with Tlp2 sensing being essential for the colonization of some plant roots and being dispensable for the colonization of the roots of others. AlphaFold structure prediction of the sensory domain of Tlp2 indicates similarity with other sensory modules in the 4HB family. The ligand binding domain represented by the Tlp2 periplasmic domain appears to be specific for a sub-group of chemoreceptors in alpha-proteobacteria, which include soil, sediment, and aquatic representatives. The 4-HB family of chemoreceptors' ligand binding domain is one of the most abundant in

completely sequenced bacterial genomes (11). This family of ligand binding domains displays responses for a range of compounds, including amino acids (32), sugars (33), di- and tri-carboxylates (34, 35), aromatic acids (36), metal ions (37), as well as inorganic phosphate (38). However, a 4HB-LBD binding nitrate has not been previously reported. Other chemoreceptors that sense nitrate and/or nitrite have been described, including the NIT domain predicted to bind nitrate (11) with experimental validation of nitrate binding in the Dd15070 chemoreceptor from *Dickeya dadantii* (39), the PacN chemoreceptor of *Pectobacterium atrosepticum,* and the PscN chemoreceptor of *Pseudomonas savastanoi* (40). The McpN chemoreceptor of *Pseudomonas aeruginosa* has an LBD annotated as a PilJ domain, and it was shown to bind nitrate and nitrite (41). However, the McpN crystal structure indicates that it does not fold as a 4HB domain (39). In all cases studied in this respect, conserved arginine residues play a critical role in nitrate (or nitrite) binding (41). Our results indicate that the conserved R159 residue of Tlp2 may be important in mediating nitrate sensing but not the R76 and R139 residues, which are also conserved. The inspection of other 4HB/ligand co-crystal structures, such as the Tar/aspartate structure, shows that amino acids from helices 1 and 4 establish direct interaction with the ligand (42, 43). Interestingly, the AlphaFold model of the Tlp2 LBD suggests that R159 is located on helix 4 and is closely related to a small kink in helix 4, which is the aspartate binding pocket in the Tar LBD. It is thus likely that R159 establishes direct interaction with the ligand. Without evidence of direct binding of nitrate to the Tlp2 LBD, the significance of these residues in the Tlp2 function remains speculative.

We suspected a role for Tlp2 in chemotaxis toward nitrate because promoter activity analyses, validated in our experiments, indicated that *tlp2* was part of the RpoN and NtrC regulons. Nitrate can be used as an alternative nitrogen source in the absence of ammonium in *A. brasilense* (25), and it can also be used as a terminal electron acceptor in the absence of oxygen (14, 44). Chemotaxis in nitrate gradients was also affected in the Δ*tlp2* strain, including under anaerobic conditions with nitrate as the sole electron acceptor. The relationship between metabolism, chemoreceptor sensory specificity, and expression level has been observed in other studies (21, 45). Similar to Tlp2, the AerC chemoreceptor is also upregulated under conditions of nitrogen fixation, and the *aerC* gene is expressed in an RpoN-dependent manner (21). These observations suggest that the chemoreceptors' composition of chemotaxis signaling arrays is remodeled under conditions of nitrogen fixation. Our findings here also suggest that combining analyses of expression patterns and metabolic considerations can be useful guides to suggest the sensory specificity of chemoreceptors.

Despite having different structural folds, nitrate has similar effects on the expression of the *P. aeruginosa* McpN chemoreceptor (41) and on that of the *A. brasilense tlp2*, namely it represses the chemoreceptor expression. This is an intriguing observation that suggests that nitrate chemotaxis must be tightly controlled by modulating the abundance of the corresponding chemoreceptors in different bacteria. In that regard, the apparent poor stability of Tlp2-YFP we observed here may be relevant to the need for a tight control of chemoreceptor abundance.

Nitrate is a key signaling molecule in plant-microbe associations, and, as noted above, several chemoreceptor ligand binding domains with specificity for nitrate have been identified in various microorganisms (39–41, 46). These ligand binding domains predicted or shown to be involved in nitrate sensing are not derived from a single common ancestor since they correspond to different structural folds, suggesting that sensing of nitrate to mediate chemotaxis responses evolved independently multiple times (11). This is not unique to nitrate sensing as many chemoreceptors with similar structural folds sense diverse and unrelated ligands (11). Conversely, structurally unrelated chemoreceptors' ligand binding domains bind similar compounds (47–51). The convergent evolution of chemoreceptors with different types of LBD that bind nitrate suggests this ligand is physiologically relevant, in particular for microorganisms that inhabit soils. Nitrate is the preferred nitrogen source available for plant nutrition, and plants have evolved multiple transport and nitrate sensing and signaling systems

(52). Nitrogen uptake rates vary depending on the plant species, and a recent study suggests that the rate of nitrogen uptake by plants modulates plant-microbe associations by competing for nitrate with rhizosphere nitrate-reducing bacteria (53). Nitrate is thus a limiting nutrient in the rhizosphere. Chemotaxis toward nitrate and dedicated chemoreceptors probably provide these motile bacteria with a competitive advantage.

The relatively small fraction of cells displaying detectable polar fluorescent foci of Tlp2-YFP is in stark contrast with the localization of other chemoreceptors we have examined under similar conditions in *A. brasilense*, where over 50% of cells typically display bright fluorescent polar foci (17, 23). This suggests that Tlp2-YFP may be present at low abundance in chemotaxis signaling arrays. Our analysis of Tlp2-YFP stability demonstrated that the protein was quite unstable and prone to degradation. Furthermore, we found that ammonium, but not nitrate, disrupted the localization of Tlp2-YFP as polar foci. This disruption was not due to an increase in protein degradation. Furthermore, a short exposure of cells to ammonium chloride for 1 hour was sufficient to decrease the fraction of cells with fluorescent polar foci of Tlp2-YFP. It is worth noting that in the 4HB LBD family (54) and the related HBM domain, ligand binding has been shown to stabilize dimerization, which is the preferred signaling state of chemoreceptors (41, 47, 55). Tlp2-YFP may be less likely to dimerize in the presence of ammonium compared to nitrate, which is its putative preferred ligand, based on the results presented here. The low abundance and intrinsic instability of this chemoreceptor make it likely that even a small change in the fraction of stable chemoreceptors would reduce the likelihood that fluorescent foci are observed. This suggests that this chemoreceptor signaling activity may depend on its expression level and the presence of its preferred ligand.

A functional Tlp2 chemoreceptor was required for root surface colonization of some of the plants tested (teff, cowpea, and red clover) but not others (wheat, sorghum, alfalfa, and pea). These findings indicate a major function for Tlp2 in the colonization of these plant roots under the conditions of our experiments. *A. brasilense* chemotaxis provides a competitive advantage in root surface colonization and most chemoreceptors characterized to date provide a competitive advantage in host root colonization, i.e., a mutant lacking a chemoreceptor displays chemotaxis defects when tested in competition with the parental strain (19, 22). It is also possible that Tlp2 would contribute to the competitive colonization of wheat, sorghum, alfalfa, or pea. The fact that a strain lacking Tlp2 is defective in root colonization of teff, cowpea, and red clover in the absence of competition suggests a major role for this chemoreceptor in this context and highlights the potential role of nitrate sensing for root surface colonization of these hosts, at least under the conditions of our experiments. This is surprising given the low abundance and instability of this chemoreceptor, but it also indicates that the role of a chemoreceptor in the colonization of a particular host plant cannot be predicted from its expression level or abundance profile. Our previous work demonstrated that chemotaxis toward plant root exudates mediates root surface colonization (22). Given the role of plant root exudates in attracting motile and chemotactic soil bacteria, the diverse composition of root exudates from diverse plants, and varying developmental stages (5, 56, 57), it is likely that teff, cowpea, and red clover produce exudates that promote bacterial sensing by Tlp2, perhaps by fostering nitrate gradient-forming conditions.

MATERIALS AND METHODS

Bacterial strains, medium, and growth conditions

The strains and plasmids used in this study are listed in Table 1. *A. brasilense* strains were grown at 28°C with shaking, in the minimal medium for *A. brasilense* (MMAB medium) supplemented with appropriate antibiotics (58). When the MMAB medium lacking a nitrogen source was used, cells were grown at 28°C without shaking to allow for microaerobic conditions that permit nitrogen fixation (59). When using solidified media, we used Noble agar because our laboratory has repeatedly observed that other sources

TABLE 1 Strains and plasmids used in this study

Strain or plasmid	Description	Source
Strains		
Sp7	Wild-type strain *Azospirillum brasilense*	ATCC 29145
Δ*tlp2*	Δ*tlp2::kan* mutant derivative of Sp7; Km^r	This work
rpoN::Km^r	*rpoN::Km* in Sp7 Km^r	(24)
ntrC::Km^r	*ntrC::Km* in Sp7 Km^r	
Δ*che1*Δ*che4*	*che1*::Km *che4*::Gm in Sp7 (Km^r Gmr)	(17)
E. coli Top10	General cloning: F– *mcrA* Δ(*mrr-hsdRMS-mcrBC*) φ80*lacZDM15* Δ*lacX74 recA1 araD139* Δ*(ara leu)7697 galU galK rpsL* (Str^r) *endA1 nupG*	Invitrogen
Plasmids		
pCR2.1-TOPO 3.9 kb	pCR2.1-TOPO 3.9 kb vector for PCR cloning; Km^r	Invitrogen
pTOPO-Tlp2	pCR2.1-TOPO with 2,269 bp fragment of *tlp2* promoter and gene; Km^r	This study
pUC19	Ap^r, general cloning vector	(60)
pRK415	*mob* + *lacZ* Tet^r	(61)
pRKTlp2^{WT}	pRK415 with HindIII/XhoI fragment of pTOPO-Tlp2; Tet^r	This study
pRKTlp2^{R159A}	pRKTlp2^{WT} with site-directed mutagenesis to obtain R159A; Tet^r	This study
pRKTlp2^{R76A}	pRKTlp2^{WT} with site-directed mutagenesis to obtain R76A; Tet^r	This study
pRKTlp2^{R139A}	pRKTlp2^{WT} with site-directed mutagenesis to obtain R139A; Tet^r	This study
pRK2013	Helper plasmid for triparental mating (ColE1 replicon; Tra Kan^r)	(62)
pRH005	Gateway-based destination vector expressing proteins fused with YFP at the C-terminus, Km^r, Cm^r	(63)
pRH-Tlp2	pRH005 containing *tlp1* ORF with the promoter region; Km^r, Cm^r	(23)
pFUS1	Broad-host-range vector with promoterless *gusA* Tet^r	(28)
pFUS-P_{tlp2}	pFUS vector containing P_{tlp2} Tet^r	This study
pFUS-P_{rpoN}	pFUS vector containing P_{rpoN} Tet^r	(64)
pFUS-P_{napA}	pFUS vector containing P_{napA} Tet^r	This study

of agar contain traces of nitrogen that inhibit the expression of nitrogen fixation genes. *Escherichia coli* strains were grown at 37°C in LB medium (yeast extract 5 g/L, tryptone 10 g/L, and NaCl 10 g/L) supplemented with appropriate antibiotics with shaking. The antibiotics were used at the following final concentrations: kanamycin [50 µg/mL for *E. coli* and 30 µg/mL for *A. brasilense*, tetracycline 10 µg/mL, ampicillin 200 µg/mL (for *A. brasilense*), and chloramphenicol (34 µg/mL for *A. brasilense*)].

Chemotaxis behavioral assays

The soft agar assay was performed as previously described (14) with minor modifications. The MMAB semi-soft agar medium [solidified with 0.3% (wt/vol) Noble agar] was supplemented with 10 or 37.5 mM of carbon source malate, succinate, or acetate. Nitrogen sources were supplemented as follows: $NaNO_3$ at a final concentration of 1, 2, 5, or 10 mM; KNO_2 at a final concentration of 5 mM; and NH_4Cl at a final concentration of 20 mM. The cultures used for the inoculation of the MMAB soft agar plates were grown in liquid MMAB medium (20 mM NH_4Cl and 37.5 mM malate) with shaking overnight at 28°C. Cells were washed three times with sterile phosphate buffer (10 mM KH_2PO_4 and 10 mM Na_2HPO_4). The optical density (OD_{600}) of the cultures was measured in the MMAB medium without nitrogen source and 37.5 mM malate and normalized to OD_{600} = 1.0, and the cultures were then incubated for 24 hours at 28°C. Next, 5 µL of cell cultures was inoculated into MMAB semi-solid medium with various nitrogen/carbon sources. The plates were incubated for 48 or 72 hours at 28°C in either aerobic or anoxic conditions, respectively. The diameter of the chemotactic rings formed after incubation was measured as previously described (14). At least three independent biological replicas were used. Anoxic conditions were produced using sealed chambers containing AnaeroPack-Anaero Anaerobic Gas Generator (Thermo Scientific Mitsubishi). The spatial gradient assays for aerotaxis were performed in a perfused chamber as

previously described (14). For the aerotaxis assay, actively growing cultures (early log phase, concentrated to OD_{600}= 1.0) were washed with 0.8% (wt/vol) sterile potassium chloride three times and resuspended in 10 mM potassium phosphate buffer, pH 7.0, supplemented with 10 mM malate (as the electron donor). Over 95% of cells are motile within the cell suspension prepared in this manner.

Complementation of Δ*tlp2* with parental and mutant genes

For functional complementation, HindIII and XhoI fragments of the *tlp2* open reading frame plus 487 bp upstream of the start codon were PCR-amplified and cloned into pCR2.1-TOPO resulting in pTOPO-Tlp2 (Table 1). A HindIII/XhoI fragment was ligated into the pRK415 vector (61) digested with the same enzymes, yielding pRKTlp2 (Table 1). pRKTlp2 was introduced into *A. brasilense* Δ*tlp2* strain by triparental mating using pRK2013 as a helper (58). Site-directed mutants of tlp2 replacing R76, R139, and R159 to alanine were generated by DNA synthesis through a commercial vendor (Genewiz, Azanta Life Sciences, USA). The *tlp2* mutants generated were then cloned into pRK415 and subsequently mated into *A. brasilense* Sp7 following a triparental mating protocol (58).

Tlp2 promoter activity and beta-glucuronidase assay

The vector pTOPO-Tlp2 (Table 1) was digested with EcoRI, and the *tlp2* fragment was purified by gel extraction (Qiagen, Valencia, CA, USA). A HindIII and PstI digestion of the purified DNA was performed to isolate a 565-bp fragment upstream of the start codon of *tlp2*. The 565-bp fragment was gel extracted and ligated into pFUS1 (28) digested with HindIII and PstI, yielding pFUS-Tlp2 (on the graphs indicated as P_{tlp2}) (Table 1). An XhoI and KpnI digestion of the purified PCR product was performed to isolate a 600-bp fragment upstream of the start codon of *napA*. The 600-bp fragment was gel extracted and ligated into pFUS1 (28) and digested with XhoI and KpnI, yielding pFUS-NapA (on the graphs indicated as P_{napA} Table 1). pFUS-Tlp2 or pFUS-NapA constructs were introduced into *A. brasilense* Sp7 through triparental mating using pRK2013 as a helper, as previously described (58). To quantitate promoter activity, the strains carrying pFUS-*tlp2* (Sp7, *ntrC*::Km, or *rpoN*::Km) were grown overnight from a single colony in the MMAB medium supplemented with tetracycline at 30°C and then re-inoculated into various media. *A. brasilense* cells were exposed to nitrogen fixation conditions for 24 hours and were spiked with different concentrations of $NaNO_3$ or NH_4Cl for 6 hours. *tlp2, rpoN,* and *napA* promoter activity was determined using the beta-glucuronidase assay using a protocol described previously (64).

Tlp2 protein localization

Δ*tlp2* strain carrying pRH005 [empty vector (63)] or pRH-Tlp2 plasmids (Table 1) was grown in an MMAB medium containing chloramphenicol for plasmid maintenance. The functionality of the Tlp2-YFP fusion was verified by complementing the Δ*tlp2* mutant chemotaxis phenotype in the soft agar plate assay. Fluorescent images of Tlp2-YFP or YFP in the Δ*tlp2* strain grown with and without shaking with 10 mM ammonium and nitrate in the nitrogen fixation conditions (after 24 hours) were taken after 6-hour spike with 10 mM nitrate, 10 mM nitrite, and 10 mM ammonium. Fluorescent images of Tlp2-YFP in the Δ*che1*Δ*che4* strain were taken after 6-hour spike with 10 mM nitrate after exposure for 24 hours to the nitrogen fixation conditions. Images of the subcellular localization of Tlp2-YFP were captured using a 100× objective with oil immersion mounted onto a Nikon fluorescent microscope. Images were collected using a 513 nm excitation argon ion laser with an emission maximum of 527 nm in the case of YFP. The total fluorescence of the cells was quantitated using ImageJ Fiji as previously described (23).

Western blot analysis

Whole-cell protein extracts were isolated as described previously (23). Briefly, 20 mL of cell cultures was used for protein isolation using sonication with the following cycles: 30 s total with 5 s ON and 10 s OFF cycle. For Western blot analysis, proteins were separated on a 10% SDS-PAGE gel and blotted onto a polyvinylidene difluoride membrane at 90 V for 1 hour 10 min. The membrane was blocked with Tris-buffered saline with 0.1% Tween 20 and 5% nonfat dry milk. YFP-tagged proteins were detected using an anti-green fluorescent protein (21) antibody at a 1:1,000 dilution. Membranes were incubated with horseradish peroxidase-conjugated secondary antibodies (anti-rabbit or anti-mouse; Abcam) at a 1:10,000 dilution and developed using a Bio-Rad imaging system. Protein abundance quantitation was performed using ImageJ Fiji.

Plant root colonization assay

Wheat (*Triticum aestivum*), sorghum (*Sorghum bicolor*), teff (*Eragrostis tef*), pea (*Pisum sativum*), cowpea (*Vigna unguiculata*), red clover (*Trifolium pratense*), and alfalfa (*Medicago sativa*) seeds were used in the root colonization assay. Plant seeds were surface sterilized for 10 min with 90% ethanol and for 15 min with a sterilization buffer containing 1% Triton X-100, 10% bleach, and sterile water. After sterilization, seeds were planted into a modified Fahreaus medium solidified with 4 g/L of Noble agar (19). All seeds were placed in the dark for 72 hours to germinate, except for pea seeds, which were germinated for 5 days. Next, the seedlings were placed into 50 mL Falcon tubes containing 15 mL of semisolid Fahreaus medium and allowed to grow for two more days. All subsequent inoculations were performed on 7-day-old germinated and surface-sterilized seedlings. For the root colonization assays, WT ev, Δ*tlp2* ev, and Δ*tlp2* Tlp2^{WT} strains of *A. brasilense* were cultured in liquid MMAB medium with 10 µg/mL (final concentration) tetracycline overnight (28°C at 175 rpm) for plasmid maintenance. The cultures were washed three times with phosphate buffer, normalized to an OD_{600} of 1.0, and further concentrated in 400 mL of the chemotaxis buffer. Twenty-five microliters of cells were injected into the medium away from the seedlings. All experiments were done in duplicate, with four biological samples used each time. One seedling of wheat, sorghum, cowpea, pea, and clover was used in each tube. Due to their very small sizes relative to other seedlings tested here, five teff seedlings per tube were used in the experiments. Plants were grown for 5 days following bacterial inoculation. After incubation, the roots were washed three times with sterile chemotaxis buffer, followed by grinding in 400 mL of the chemotaxis buffer. The ground roots' supernatant was serially diluted and plated onto MMAB medium with 10 µg/mL (final concentration) tetracycline for CFU counts, which were performed after 48 hours of incubation at 28°C. Root colonization efficiency was calculated as follows: ln [CFU (t_5 roots)/CFU (t_0)/g of wet roots], where t_5 is the time at which plants were sacrificed, 5 days post-inoculation and t_0 was the time of initial bacterial inoculation. The cells remaining in the medium surrounding the roots were also counted by determining CFU in the medium, calculated as follows: ln [CFU (t_5 medium)/CFU (t_0)/g of medium]. This control was performed to ensure that the strains inoculated had no growth or viability impairment or advantage that could confound the inoculation results.

Protein sequence and phylogenetic analysis

A similarity search against the non-redundant database was performed using the PSI-BLAST (65) with residues 42–193 of Tlp2 as the query. Domain architecture was analyzed using the AlphaFold and ChimeraX software (66, 67).

ACKNOWLEDGMENTS

The authors thank Tino Krell and Brittany Belin for excellent suggestions that greatly improved the manuscript and the Advanced Microscopy and Imaging Center, University of Tennessee, Knoxville, for assistance.

This research was supported by the National Science Foundation grant NSF-MCB 2130556 (to G.A.). Any opinions, findings, conclusions, or recommendations expressed in this material are those of the authors and do not necessarily reflect the views of the National Science Foundation.

AUTHOR AFFILIATION

[1]Biochemistry and Cellular and Molecular Biology Department, University of Tennessee, Knoxville, Tennessee, USA

AUTHOR ORCIDs

Gladys Alexandre http://orcid.org/0000-0002-9238-4640

FUNDING

Funder	Grant(s)	Author(s)
National Science Foundation (NSF)	MCB 2130556	Gladys Alexandre

AUTHOR CONTRIBUTIONS

Elena E. Ganusova, Conceptualization, Data curation, Formal analysis, Investigation, Supervision, Writing – original draft, Writing – review and editing | Matthew H. Russell, Conceptualization, Data curation, Investigation | Siddhi Patel, Investigation | Terry Seats, Investigation | Gladys Alexandre, Conceptualization, Formal analysis, Funding acquisition, Project administration, Writing – review and editing

DIRECT CONTRIBUTION

This article is a direct contribution from Gladys Alexandre, a member of the *Applied and Environmental Microbiology* Editorial Board, who arranged for and secured reviews by Brittany Belin, Carnegie Institution for Science, and Tino Krell, Estacion Experimental del Zaidin - CSIC.

ADDITIONAL FILES

The following material is available online.

Supplemental Material

Supplemental material (AEM00760-24-s0001.pdf). Table S1; Fig. S1 to S7.

REFERENCES

1. Pereg L, de-Bashan LE, Bashan Y. 2016. Assessment of affinity and specificity of *Azospirillum* for plants. Plant Soil 399:389–414. https://doi.org/10.1007/s11104-015-2778-9
2. Fukami J, Cerezini P, Hungria M. 2018. *Azospirillum*: benefits that go far beyond biological nitrogen fixation. AMB Express 8:73. https://doi.org/10.1186/s13568-018-0608-1
3. Buchan A, Crombie B, Alexandre GM. 2010. Temporal dynamics and genetic diversity of chemotactic-competent microbial populations in the rhizosphere. Environ Microbiol 12:3171–3184. https://doi.org/10.1111/j.1462-2920.2010.02290.x
4. Scharf BE, Hynes MF, Alexandre GM. 2016. Chemotaxis signaling systems in model beneficial plant-bacteria associations. Plant Mol Biol 90:549–559. https://doi.org/10.1007/s11103-016-0432-4
5. O'Banion BS, O'Neal L, Alexandre G, Lebeis SL. 2020. Bridging the gap between single-strain and community-level plant-microbe chemical interactions. Mol Plant Microbe Interact 33:124–134. https://doi.org/10.1094/MPMI-04-19-0115-CR
6. Falke JJ, Bass RB, Butler SL, Chervitz SA, Danielson MA. 1997. The two-component signaling pathway of bacterial chemotaxis: a molecular view of signal transduction by receptors, kinases, and adaptation enzymes. Annu Rev Cell Dev Biol 13:457–512. https://doi.org/10.1146/annurev.cellbio.13.1.457
7. Porter SL, Wadhams GH, Armitage JP. 2011. Signal processing in complex chemotaxis pathways. Nat Rev Microbiol 9:153–165. https://doi.org/10.1038/nrmicro2505
8. Yang W, Briegel A. 2020. Diversity of bacterial chemosensory arrays. Trends Microbiol 28:68–80. https://doi.org/10.1016/j.tim.2019.08.002
9. Sourjik V, Armitage JP. 2010. Spatial organization in bacterial chemotaxis. EMBO J 29:2724–2733. https://doi.org/10.1038/emboj.2010.178
10. Hazelbauer GL, Falke JJ, Parkinson JS. 2008. Bacterial chemoreceptors: high-performance signaling in networked arrays. Trends Biochem Sci 33:9–19. https://doi.org/10.1016/j.tibs.2007.09.014
11. Ortega Á, Zhulin IB, Krell T. 2017. Sensory repertoire of bacterial chemoreceptors. Microbiol Mol Biol Rev 81:e00033-17. https://doi.org/10.1128/MMBR.00033-17
12. Matilla MA, Martín-Mora D, Krell T. 2020. The use of isothermal titration calorimetry to unravel chemotactic signalling mechanisms. Environ Microbiol 22:3005–3019. https://doi.org/10.1111/1462-2920.15035

13. Zhulin IB, Bespalov VA, Johnson MS, Taylor BL. 1996. Oxygen taxis and proton motive force in *Azospirillum brasilense*. J Bacteriol 178:5199–5204. https://doi.org/10.1128/jb.178.17.5199-5204.1996
14. Alexandre G, Greer SE, Zhulin IB. 2000. Energy taxis is the dominant behavior in *Azospirillum brasilense*. J Bacteriol 182:6042–6048. https://doi.org/10.1128/JB.182.21.6042-6048.2000
15. Mukherjee T, Kumar D, Burriss N, Xie Z, Alexandre G. 2016. *Azospirillum brasilense* chemotaxis depends on two signaling pathways regulating distinct motility parameters. J Bacteriol 198:1764–1772. https://doi.org/10.1128/JB.00020-16
16. Wisniewski-Dyé F, Borziak K, Khalsa-Moyers G, Alexandre G, Sukharnikov LO, Wuichet K, Hurst GB, McDonald WH, Robertson JS, Barbe V, et al. 2011. *Azospirillum* genomes reveal transition of bacteria from aquatic to terrestrial environments. PLoS Genet 7:e1002430. https://doi.org/10.1371/journal.pgen.1002430
17. O'Neal L, Gullett JM, Aksenova A, Hubler A, Briegel A, Ortega D, Kjær A, Jensen G, Alexandre G. 2019. Distinct chemotaxis protein paralogs assemble into chemoreceptor signaling arrays to coordinate signaling output. mBio 10:e01757-19. https://doi.org/10.1128/mBio.01757-19
18. Gumerov VM, Ulrich LE, Zhulin IB. 2024. MiST 4.0: a new release of the microbial signal transduction database, now with a metagenomic component. Nucleic Acids Res 52:D647–D653. https://doi.org/10.1093/nar/gkad847
19. Greer-Phillips SE, Stephens BB, Alexandre G. 2004. An energy taxis transducer promotes root colonization by *Azospirillum brasilense*. J Bacteriol 186:6595–6604. https://doi.org/10.1128/JB.186.19.6595-6604.2004
20. Russell MH, Bible AN, Fang X, Gooding JR, Campagna SR, Gomelsky M, Alexandre G. 2013. Integration of the second messenger c-di-GMP into the chemotactic signaling pathway. mBio 4:e00001-13. https://doi.org/10.1128/mBio.00001-13
21. Xie Z, Ulrich LE, Zhulin IB, Alexandre G. 2010. PAS domain containing chemoreceptor couples dynamic changes in metabolism with chemotaxis. Proc Natl Acad Sci U S A 107:2235–2240. https://doi.org/10.1073/pnas.0910055107
22. O'Neal L, Akhter S, Alexandre G. 2019. A PilZ-containing chemotaxis receptor mediates oxygen and wheat root sensing in *Azospirillum brasilense*. Front Microbiol 10:312. https://doi.org/10.3389/fmicb.2019.00312
23. Ganusova EE, Rost M, Aksenova A, Abdulhussein M, Holden A, Alexandre G. 2023. *Azospirillum brasilense* AerC and Tlp4b cytoplasmic chemoreceptors are promiscuous and interact with the two membrane-bound chemotaxis signaling clusters mediating chemotaxis responses. J Bacteriol 205:e0048422. https://doi.org/10.1128/jb.00484-22
24. Milcamps A, Van Dommelen A, Stigter J, Vanderleyden J, de Bruijn FJ. 1996. The *Azospirillum brasilense rpoN* gene is involved in nitrogen fixation, nitrate assimilation, ammonium uptake, and flagellar biosynthesis. Can J Microbiol 42:467–478. https://doi.org/10.1139/m96-064
25. Van Dommelen A, Keijers V, Vanderleyden J, de Zamaroczy M. 1998. (Methyl)ammonium transport in the nitrogen-fixing bacterium *Azospirillum brasilense*. J Bacteriol 180:2652–2659. https://doi.org/10.1128/JB.180.10.2652-2659.1998
26. Solovyev VV, SalamovAA. Automatic annotation of microbial genomes and metagenomic sequences 3 MATERIAL AND METHODS learning parameters and prediction of protein-coding genes
27. Sun L, Ataka M, Kominami Y, Yoshimura K, Kitayama K. 2021. A constant microbial C/N ratio mediates the microbial nitrogen mineralization induced by root exudation among four co-existing canopy species. Rhizosphere 17:100317. https://doi.org/10.1016/j.rhisph.2021.100317
28. Revers LF, Passaglia LM, Marchal K, Frazzon J, Blaha CG, Vanderleyden J, Schrank IS. 2000. Characterization of an *Azospirillum brasilense* Tn5 mutant with enhanced N(2) fixation: the effect of ORF280 on nifH expression. FEMS Microbiol Lett 183:23–29. https://doi.org/10.1111/j.1574-6968.2000.tb08928.x
29. Liang YY, Arsène F, Elmerich C. 1993. Characterization of the ntrBC genes of *Azospirillum brasilense* Sp7: their involvement in the regulation of nitrogenase synthesis and activity. Mol Gen Genet 240:188–196. https://doi.org/10.1007/BF00277056
30. Steenhoudt O, Keijers V, Okon Y, Vanderleyden J. 2001. Identification and characterization of a periplasmic nitrate reductase in *Azospirillum brasilense* Sp245. Arch Microbiol 175:344–352. https://doi.org/10.1007/s002030100271
31. Okon Y, Itzigsohn R. 1992. Poly-β-hydroxybutyrate metabolism in *Azospirillum brasilense* and the ecological role of PHB in the rhizosphere. FEMS Microbiol Rev 103:131–139. https://doi.org/10.1111/j.1574-6968.1992.tb05830.x
32. Springer MS, Goy MF, Adler J. 1977. Sensory transduction in *Escherichia coli*: two complementary pathways of information processing that involve methylated proteins. Proc Natl Acad Sci U S A 74:3312–3316. https://doi.org/10.1073/pnas.74.8.3312
33. Harayama S, Palva ET, Hazelbauer GL. 1979. Transposon-insertion mutants of *Escherichia coli* K12 defective in a component common to galactose and ribose chemotaxis. Mol Gen Genet 171:193–203. https://doi.org/10.1007/BF00270005
34. Milligan DL, Koshland DE. 1993. Purification and characterization of the periplasmic domain of the aspartate chemoreceptor. Journal of Biological Chemistry 268:19991–19997. https://doi.org/10.1016/S0021-9258(20)80684-X
35. Biemann HP, Koshland DE. 1994. Aspartate receptors of *Escherichia coli* and *Salmonella typhimurium* bind ligand with negative and half-of-the-sites cooperativity. Biochemistry 33:629–634. https://doi.org/10.1021/bi00169a002
36. Li Y, Liang J, Yang S, Yao J, Chen K, Yang L, Zheng W, Tian Y. 2021. Finding novel chemoreceptors that specifically sense and trigger chemotaxis toward polycyclic aromatic hydrocarbons in *Novosphingobium pentaromativorans* US6-1. J Hazard Mater 416:126246. https://doi.org/10.1016/j.jhazmat.2021.126246
37. Tso WW, Adler J. 1974. Negative chemotaxis in *Escherichia coli*. J Bacteriol 118:560–576. https://doi.org/10.1128/jb.118.2.560-576.1974
38. Francis VI, Stevenson EC, Porter SL. 2017. Two-component systems required for virulence in *Pseudomonas aeruginosa*. FEMS Microbiol Lett 364:fnx104. https://doi.org/10.1093/femsle/fnx104
39. Gálvez-Roldán C, Cerna-Vargas JP, Rodríguez-Herva JJ, Krell T, Santamaría-Hernando S, López-Solanilla E. 2023. A nitrate-sensing domain-containing chemoreceptor is required for successful entry and virulence of *Dickeya dadantii* 3937 in potato plants. Phytopathology 113:390–399. https://doi.org/10.1094/PHYTO-10-22-0367-R
40. Monteagudo-Cascales E, Ortega Á, Velando F, Morel B, Matilla MA, Krell T. 2023. Study of NIT domain-containing chemoreceptors from two global phytopathogens and identification of NIT domains in eukaryotes. Mol Microbiol 119:739–751. https://doi.org/10.1111/mmi.15069
41. Martín-Mora D, Ortega Á, Matilla MA, Martínez-Rodríguez S, Gavira JA, Krell T. 2019. The molecular mechanism of nitrate chemotaxis via direct ligand binding to the PilJ domain of McpN. mBio 10:e02334-18. https://doi.org/10.1128/mBio.02334-18
42. Milburn MV, Privé GG, Milligan DL, Scott WG, Yeh J, Jancarik J, Koshland DE, Kim SH. 1991. Three-dimensional structures of the ligand-binding domain of the bacterial aspartate receptor with and without a ligand. Science 254:1342–1347. https://doi.org/10.1126/science.1660187
43. Mise T. 2016. Structural analysis of the ligand-binding domain of the aspartate receptor tar from *Escherichia coli*. Biochemistry 55:3708–3713. https://doi.org/10.1021/acs.biochem.6b00160
44. Tarrand JJ, Krieg NR, Döbereiner J. 1978. A taxonomic study of the *Spirillum lipoferum* group, with descriptions of a new genus, *Azospirillum* gen. nov. and two species, *Azospirillum lipoferum* (Beijerinck) comb. nov. and *Azospirillum brasilense* sp. nov. Can J Microbiol 24:967–980. https://doi.org/10.1139/m78-160
45. López-Farfán D, Reyes-Darias JA, Krell T. 2017. The expression of many chemoreceptor genes depends on the cognate chemoeffector as well as on the growth medium and phase. Curr Genet 63:457–470. https://doi.org/10.1007/s00294-016-0646-7
46. Shu CJ, Ulrich LE, Zhulin IB. 2003. The NIT domain: a predicted nitrate-responsive module in bacterial sensory receptors. Trends Biochem Sci 28:121–124. https://doi.org/10.1016/S0968-0004(03)00032-X
47. Lacal J, García-Fontana C, Muñoz-Martínez F, Ramos JL, Krell T. 2010. Sensing of environmental signals: classification of chemoreceptors according to the size of their ligand binding regions. Environ Microbiol 12:2873–2884. https://doi.org/10.1111/j.1462-2920.2010.02325.x
48. Parkinson JS, Hazelbauer GL, Falke JJ. 2015. Signaling and sensory adaptation in *Escherichia coli* chemoreceptors: 2015 update. Trends Microbiol 23:257–266. https://doi.org/10.1016/j.tim.2015.03.003

49. Boyeldieu A, Poli JP, Ali Chaouche A, Fierobe HP, Giudici-Orticoni MT, Méjean V, Jourlin-Castelli C. 2022. Multiple detection of both attractants and repellents by the dCache-chemoreceptor SO_1056 of *Shewanella oneidensis*. FEBS J 289:6752–6766. https://doi.org/10.1111/febs.16548
50. Velando F, Matilla MA, Zhulin IB, Krell T. 2023. Three unrelated chemoreceptors provide *Pectobacterium atrosepticum* with a broad-spectrum amino acid sensing capability. Microb Biotechnol 16:1548–1560. https://doi.org/10.1111/1751-7915.14255
51. Dlakić M. 2023. Discovering unknown associations between prokaryotic receptors and their ligands. Proc Natl Acad Sci U S A 120:e2316830120. https://doi.org/10.1073/pnas.2316830120
52. Vidal EA, Alvarez JM, Araus V, Riveras E, Brooks MD, Krouk G, Ruffel S, Lejay L, Crawford NM, Coruzzi GM, Gutiérrez RA. 2020. Nitrate in 2020: thirty years from transport to signaling networks. Plant Cell 32:2094–2119. https://doi.org/10.1105/tpc.19.00748
53. Moreau D, Pivato B, Bru D, Busset H, Deau F, Faivre C, Matejicek A, Strbik F, Philippot L, Mougel C. 2015. Plant traits related to nitrogen uptake influence plant-microbe competition. Ecology 96:2300–2310. https://doi.org/10.1890/14-1761.1
54. Guo L, Wang YH, Cui R, Huang Z, Hong Y, Qian JW, Ni B, Xu AM, Jiang CY, Zhulin IB, Liu SJ, Li DF. 2023. Attractant and repellent induce opposing changes in the four-helix bundle ligand-binding domain of a bacterial chemoreceptor. PLoS Biol 21:e3002429. https://doi.org/10.1371/journal.pbio.3002429
55. Rico-Jiménez M, Muñoz-Martínez F, García-Fontana C, Fernandez M, Morel B, Ortega A, Ramos JL, Krell T. 2013. Paralogous chemoreceptors mediate chemotaxis towards protein amino acids and the non-protein amino acid gamma-aminobutyrate (GABA). Mol Microbiol 88:1230–1243. https://doi.org/10.1111/mmi.12255
56. Upadhyay SK, Srivastava AK, Rajput VD, Chauhan PK, Bhojiya AA, Jain D, Chaubey G, Dwivedi P, Sharma B, Minkina T. 2022. Root exudates: mechanistic insight of plant growth promoting rhizobacteria for sustainable crop production. Front Microbiol 13:916488. https://doi.org/10.3389/fmicb.2022.916488
57. Pantigoso HA, Newberger D, Vivanco JM. 2022. The rhizosphere microbiome: plant-microbial interactions for resource acquisition. J Appl Microbiol 133:2864–2876. https://doi.org/10.1111/jam.15686
58. Hauwaerts D, Alexandre G, Das SK, Vanderleyden J, Zhulin IB. 2002. A major chemotaxis gene cluster in *Azospirillum brasilense* and relationships between chemotaxis operons in alpha-proteobacteria. FEMS Microbiol Lett 208:61–67. https://doi.org/10.1111/j.1574-6968.2002.tb11061.x
59. Baldani JI, Reis VM, Videira SS, Boddey LH, Baldani VLD. 2014. The art of isolating nitrogen-fixing bacteria from non-leguminous plants using N-free semi-solid media: a practical guide for microbiologists. Plant Soil 384:413–431. https://doi.org/10.1007/s11104-014-2186-6
60. Yanisch-Perron C, Vieira J, Messing J. 1985. Improved M13 phage cloning vectors and host strains: nucleotide sequences of the M13mp18 and pUC19 vectors. Gene 33:103–119. https://doi.org/10.1016/0378-1119(85)90120-9
61. Keen NT, Tamaki S, Kobayashi D, Trollinger D. 1988. Improved broad-host-range plasmids for DNA cloning in Gram-negative bacteria. Gene 70:191–197. https://doi.org/10.1016/0378-1119(88)90117-5
62. Figurski DH, Helinski DR. 1979. Replication of an origin-containing derivative of plasmid RK2 dependent on a plasmid function provided in trans. Proc Natl Acad Sci U S A 76:1648–1652. https://doi.org/10.1073/pnas.76.4.1648
63. Hallez R, Letesson J-J, Vandenhaute J, De Bolle X. 2007. Gateway-based destination vectors for functional analyses of bacterial ORFeomes: application to the min system in *Brucella abortus*. Appl Environ Microbiol 73:1375–1379. https://doi.org/10.1128/AEM.01873-06
64. Ganusova EE, Vo LT, Abraham PE, O'Neal Yoder L, Hettich RL, Alexandre G. 2021. The *Azospirillum brasilense* core chemotaxis proteins CheA1 and CheA4 link chemotaxis signaling with nitrogen metabolism. mSystems 6:e01354-20. https://doi.org/10.1128/mSystems.01354-20
65. Altschul SF, Madden TL, Schäffer AA, Zhang J, Zhang Z, Miller W, Lipman DJ. 1997. Gapped BLAST and PSI-BLAST: a new generation of protein database search programs. Nucleic Acids Res 25:3389–3402. https://doi.org/10.1093/nar/25.17.3389
66. Jumper J, Evans R, Pritzel A, Green T, Figurnov M, Ronneberger O, Tunyasuvunakool K, Bates R, Žídek A, Potapenko A, et al. 2021. Highly accurate protein structure prediction with AlphaFold. Nature 596:583–589. https://doi.org/10.1038/s41586-021-03819-2
67. Meng EC, Goddard TD, Pettersen EF, Couch GS, Pearson ZJ, Morris JH, Ferrin TE. 2023. UCSF ChimeraX: tools for structure building and analysis. Protein Sci 32:e4792. https://doi.org/10.1002/pro.4792